**Title:** Advanced Hydrogen Transport Membranes for Vision 21 Fossil Fuel Plants

**Type of Report:** Quarterly

**Reporting Period Start Date:** October 1, 2000

**Reporting Period End Date:** January 1, 2001

**Principal Authors:** Shane E. Roark, Tony F. Sammells, Adam Calihman, Andy Girard, Pamela M. Van Calcar, Richard Mackay, Tom Barton, Sara Rolfe

**Date Report was Issued:** January 30, 2001

**DOE Award Number:** DE-FC26-00NT40762

**Name and Address of Submitting Organization:**
Eltron Research Inc., 4600 Nautilus Court South, Boulder, CO 80301-3241

## DISCLAIMER

## ABSTRACT

Eltron Research Inc., and team members CoorsTek, McDermott Technology, Inc., Süd Chemie, Argonne National Laboratory, and Oak Ridge National Laboratory are developing an environmentally benign, inexpensive, and efficient method for separating hydrogen from gas mixtures produced during industrial processes, such as coal gasification. This objective is being pursued using dense membranes based in part on Eltron-patented ceramic materials with a demonstrated ability for proton and electron conduction. The technical goals are being addressed by modifying single-phase and composite membrane composition and microstructure to maximize proton and electron conductivity without loss of material stability. Ultimately, these materials must enable hydrogen separation at practical rates under ambient and high-pressure conditions, without deactivation in the presence of feedstream components such as carbon dioxide, water, and sulfur.

This project was motivated by the National Energy Technology Laboratory (NETL) Vision 21 initiative which seeks to economically eliminate environmental concerns associated with the use of fossil fuels. The proposed technology addresses the DOE Vision 21 initiative in two ways. First, this process offers a relatively inexpensive solution for pure hydrogen separation that can be easily incorporated into Vision 21 fossil fuel plants. Second, this process could reduce the cost of hydrogen, which is a clean burning fuel under increasing demand as supporting technologies are developed for hydrogen utilization and storage. Additional motivation for this project arises from the potential of this technology for other applications.

Membranes testing during this reporting period were greater than 1 mm thick and had the general perovskite composition $AB_{1-x}B'_xO_{3-\delta}$, where $0.05 \le x \le 0.3$. These materials demonstrated hydrogen separation rates between 1 and 2 mL/min/cm$^2$, which represents roughly 20% of the target goal for membranes of this thickness. The sintered membranes were greater than 95% dense, but the phase purity decreased with increasing dopant concentration. The quantity of dopant incorporated into the perovskite phase was roughly constant, with excess dopant forming an additional phase. Composite materials with distinct ceramic and metallic phases, and thin film perovkites (100 µm) also were successfully prepared, but have not yet been tested for hydrogen transport. Finally, porous platinum was identified as a excellent catalyst for evaluation of membrane materials, however, lower cost nickel catalyst systems are being developed.

## INTRODUCTION

The objective of this project is to develop an environmentally benign, inexpensive, and efficient method for separating hydrogen from gas mixtures produced during industrial processes, such as coal gasification. This objective will be accomplished by employing dense ceramic and composite membranes based in part on Eltron-patented materials (Patent No. US5821185) with a demonstrated ability for rapid proton and electron conduction. The primary technical challenge in achieving the goals of this project will be to optimize membrane composition and microstructure to enable practical hydrogen separation rates and chemical stability. Other key aspects of this developing technology include catalysis, ceramic processing methods, and separation unit design operating under high pressure. To achieve these technical goals, Eltron Research, Inc. has organized a consortium consisting of CoorsTek, McDermott Technology, Inc., Süd Chemie, Argonne National Laboratory, and Oak Ridge National Laboratory.

The process for hydrogen separation using a dense perovskite-based ceramic membrane is shown schematically in Figure 1. In this example, a syngas mixture ($CO_2$, CO, and $H_2$) is passed across the membrane surface where hydrogen is oxidized catalytically. The protons and electrons generated are incorporated into the membrane material lattice and conducted to the reduction surface where the reverse reduction reaction occurs to produce pure hydrogen. It is anticipated that this approach for hydrogen separation will provide the following benefits: i) Since the membrane materials are inexpensive and are mixed proton and electronic conductors, the system design is inherently simple and economical, requiring no external circuitry or applied potential. ii) Because the membranes are nonporous, only hydrogen will be transported through the membrane, without contributions from break-through of other gases. Accordingly, the separated hydrogen will be of high purity, and these high-density membranes are not subject to problems associated with pore clogging. iii) The conduction mechanism in these materials occurs at elevated temperatures compatible with incorporation into chemical processing streams. And, iv) in addition to hydrogen separation, this ceramic membrane technology can be used to facilitate numerous chemical processing applications.

The overall approach for this project is divided into three categories: i) optimization of perovskite compositions for high mixed proton and electron conductivity and stability, ii) development of multi-phase materials, and iii) fabrication of supported thin ceramic films. Each category will be pursued concurrently throughout the program. However, in the very early stages effort will focus on generating a database of relevant material properties as a function of ceramic composition and preparation. This database will enable strategic selection of membrane components for optimizing performance.

During this reporting period the majority of effort was directed toward

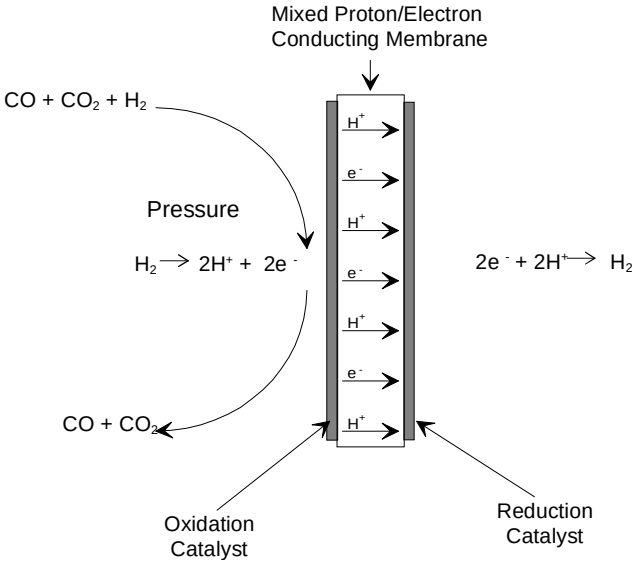


**Figure 1. Schematic diagram of the hydrogen separation process using a dense ceramic membrane.**

construction of apparatuses for ambient and high-pressure membrane screening, as well as development and confirmation of membrane evaluation methodology. These tasks will be described below in addition to preliminary transport and conductivity measurements for some simple doped perovskite ceramics.

## EXPERIMENTAL

### a. Preparation of Ceramic Powders

Ceramic powders were prepared by combining oxide precursors in the appropriate stoichiometric ratio with several yttria-stabilized zirconia (YSZ) grinding media. The mixtures were thoroughly ground by ball milling for approximately 24 hours, then passed through a 355-µm sieve, and placed in an alumina crucible for calcination to achieve the desired perovskite composition. Samples were calcined between 1200° and 1400°C for approximately 6 hours in air, then again sieved to 355 µm. Powder particle size was reduced by attrition using a Union Process Model 01 Attritor with a MgO-stabilized zirconia tank and plastic agitator arms. Spherical YSZ grinding media and isopropanol were included in the tank during attrition to promote grinding of the precursor powders. After attrition, isopropanol was evaporated, and powders were passed through, respectively, 355-µm, 90-µm, and 38-µm sieves.

### b. Preparation of Composite Materials

During this reporting period, composite materials were prepared by mixing appropriate ratios of proton or mixed proton/electron conducting ceramics with metal or electron conducting metal oxide powders. The mixtures were combined with 2 wt.-% Ceracer630 binder (Shamrock) and ball milled for 2 hours in acetone. After drying, the powders were sieved through a #170 mesh. Pellets of the materials were pressed at 20,000 lbs, then sintered at 1475°C for 4 to 6 hours in either air or $H_2$/He, depending on composition.

### c. Fabrication of Tube and Disk Membranes

Tubular membranes with one closed end were prepared from the powders described above. The general procedure was to obtain an appropriate weight of the powder materials and add 2 wt.% of polyvinyl butyral (PVB) binder using isopropanol as a solvent. The solvent was evaporated from the powder/binder mixtures, and the powders were passed in series through 355-µm, 90-µm, and 38-µm sieves. Ceramic membrane tubes were prepared by molding under isostatic pressure using a Fluitron CP2-10-60 isostatic press. For each tube, the necessary amount of powder (usually ~10 g) was poured into a rubber mold (Trexler Rubber Co.) containing a stainless steel mandrel. The assembly was placed into the isostatic press, de-aerated by vacuum, and formed at 20,000 psi for 2 minutes. After depressurization, the mold was removed from the press, and the 'green' tube removed from the mold. Tubes were placed on a bed of powder of the same composition in a ceramic boat (Coors Ceramics) and the binder material was burned out by heating in air at 1°C/min to 600°C. Tubes then were heated at 3°C/min to the desired sintering temperature and maintained for 4 hours, followed by cooling to 500°C at 1°C/min, then to room temperature at 5°/min. The

sintering temperatures were between 1400°C and 1600°C. Densities were measured using the Archemedies method.

Disk membranes were prepared by pouring ~2 g of material powder into a die, and pressing uniaxially at 15,000 psi for ~30 seconds. The disks were sintered as described above, and had diameters of ~10 mm and a thickness between 1 and 5 mm.

### d. Construction and Operation of Conductivity Apparatus

Measurements of membrane proton and electron conductivity proceeded by incorporating disk membranes into an electrochemical cell represented by $H_2$ (1 atm)/Pt/Ceramic Membrane/Pt/Ar, $H_2$ (<<1 atm). A diagram of the cell is shown in Figure 2, and a photograph of the apparatus is shown in Figure 3. Pt ink (Heraeus) was used to screen print porous Pt electrodes onto each side of the disks. Pt leads (Alpha Omega) were attached to each surface using Ag epoxy (SPI, inc.). To seal the disks in the reactor, Pyrex rings were positioned between the disks and tubing, and the assembly heated past the Pyrex softening temperature (> 850°C) under a spring-loaded pressure. The cell temperature was controlled by a furnace, and gases were supplied through needle valve flow meters. Electrochemical measurements were recorded across leads extending from the ends of the reactor using a Hewlett-Packard 34970A Data Acquisition/Switch Unit.

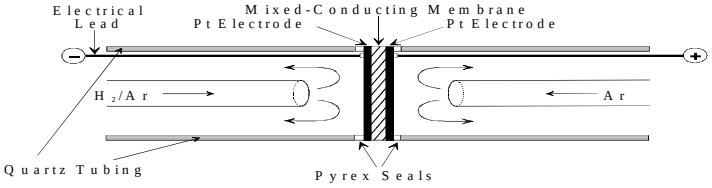


**Figure 2. Diagram of the electrochemical cell used for measurement of proton and electron conductivity of membrane materials.**

**Figure 3. Photograph of the apparatus used for measurement of membrane proton and electron conductivity.**

Conductivity measurements were acquired using a $H_2$ concentration gradient across the membrane. The gradient was established by flowing pure $H_2$ on one side and only Ar on the other. The $H_2$ transported to the Ar side was measured using gas chromatography, and the resulting transport potential, *E*, was calculated from the Nernst equation,

$$E = -\frac{RT}{2F}\ln\frac{\left[H_2^{'}\right]}{\left[H_2\right]} \qquad (1)$$

where $R$ is the Gas Constant, $T$ is temperature, $F$ is the Faraday Constant, and $[H_2']/[H_2]$ is the ratio of the dilute to concentrated side. The ionic transfer number was calculated from $E$ and the measured open cell voltage, $OCV$, according to,

$$t_i = \frac{OCV}{E} \tag{2}$$

The membrane total resistance, $R_m$, was determined from the slope of cell voltage, $V$, versus current, $I$, curves prepared for a range of ten precision resistors included in the circuit. The membrane total conductivity, $\sigma_m$, was calculated from,

$$\sigma_m = \frac{d}{AR_m} \tag{4}$$

where $d$ is the membrane thickness and $A$ is the area on one side. Finally, the ionic conductivity, $\sigma_i$, was calculated from,

$$\sigma_i = t_i \sigma_m \tag{5}$$

and the electron conductivity, $\sigma_e$, was calculated from,

$$\sigma_e = (1 - t_i)\sigma_m \tag{6}$$

These experiments were repeated over a temperature range of ~600° to 900°C, and the activation energy for proton and electron conduction, $E_a$, was determined from Arrhenius-type plots according to,

$$\sigma_{i,e} \propto \frac{1}{T} \exp\left(\frac{-E_a}{kT}\right) \tag{7}$$

where $T$ is temperature and $k$ is the Boltzmann Constant.

### e. Construction and Operation of Ambient Pressure Hydrogen Separation Units

The conductivity apparatus described above was used exclusively to determine transport rates for disk membranes, and four new units were constructed for tube membrane evaluation. A schematic diagram for two tube membrane evaluation units is shown in Figure 4, and a photograph is shown in Figure 5. The hydrogen-separation cells are positioned inside the furnaces using

appropriate Swagelok fittings to join the quartz tubing to stainless steel inlet and outlet tubing. The concentrations of the constituents of the inlet hydrogen-rich gas stream (*e.g.*, syngas) were adjusted at a flow control manifold, then introduced through the top of the separation cell. Humidity can be introduced by flowing the gas through a temperature-controlled water bubbler, and measured using an in-line humidity sensor. A diagram of the hydrogen separation cell is shown in Figure 6. The seal between the membrane and alumina cup was formed by heating crushed Pyrex above the melting temperature under a flow of argon. The hydrogen inlet stream is passed through the separation cell, where hydrogen is transferred across the membrane into the sweep chamber. Argon sweep gas enters the sweep chamber through an inner gas line concentric with a larger exit line, and the separated hydrogen and sweep gas exit the cell through the outside exit line. Sampling of inlet and outlet streams was achieved through ports located just outside the furnaces. Flow rates for the evaluations were between 30 and 100 mL/min on each side of the membrane.

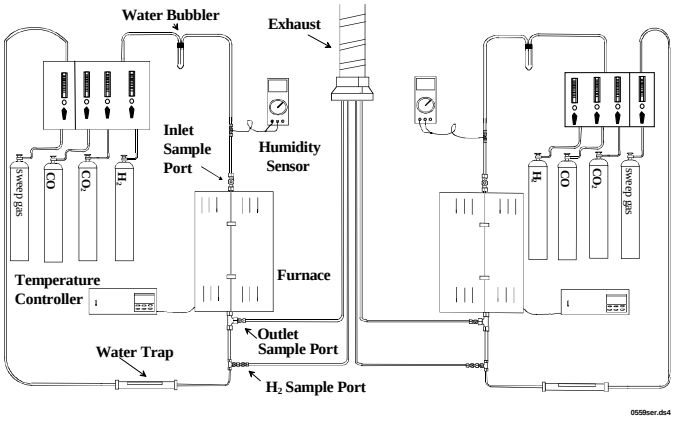


**Figure 4. Schematic diagram of the apparatus for hydrogen separation membrane evaluation.**

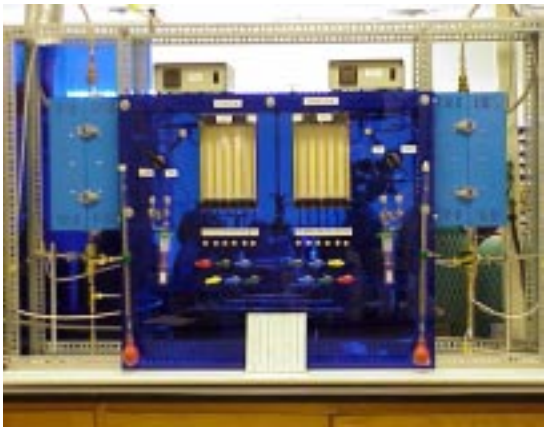

**Figure 5. Photograph of the apparatus for hydrogen separation membrane evaluation.**

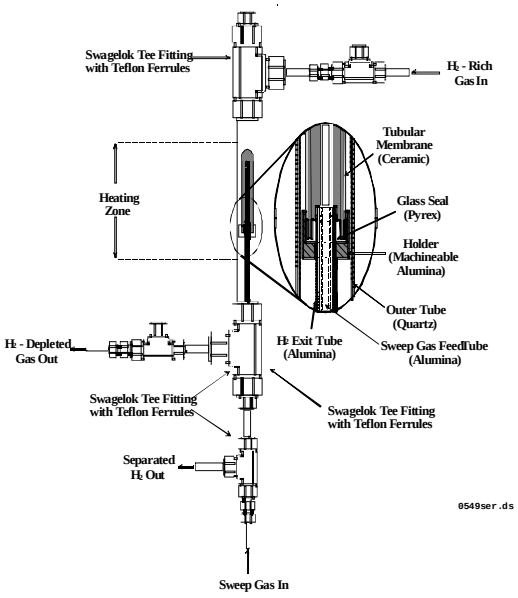


**Figure 6. Schematic diagram of the hydrogen separation cell.**

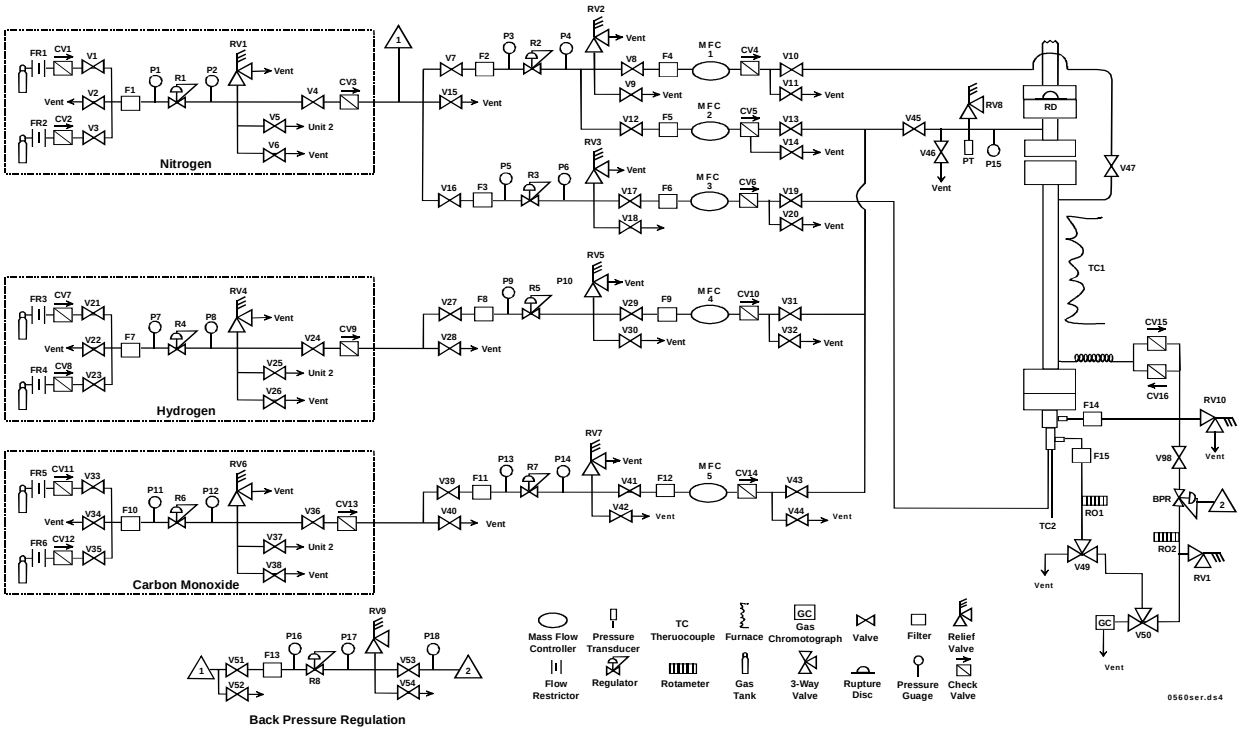


**Figure 7. Schematic diagram of the apparatus for evaluation of hydrogen separation membranes at high pressure.**

### f. Construction of High Pressure Hydrogen Separation Units

Construction of the high pressure hydrogen separation units recently was completed, and was much more involved than the ambient pressure units. A schematic diagram is shown in Figure 7 and a photograph is shown in Figure 8. Support hardware consists of devices for gas supply and mixing, plus analytical instruments to monitor products. The nitrogen supply system performs four functions. First, nitrogen is used to pressurize the separation vessel and dilute the syngas feedstream. Second, the space between the vessel liner and the vessel wall is purged with nitrogen to prevent interaction of carbon monoxide with Haynes 230 alloy at elevated temperatures. Third, nitrogen is used as the sweep gas to remove hydrogen transported through the ceramic membrane. Fourth, nitrogen is used to load the back pressure regulator. The supply manifold for nitrogen consists of two or more 6000-psig tanks, CGAs fitted with flow restrictors, check valves, shutoff valves, and a vent valve. From the


**Figure 8. Photograph of the apparatus for evaluation of hydrogen separation membranes at high pressure.**

manifold, the gas flows through a filter to a regulator where the pressure is reduced to near operational pressure. A 450-psig relief valve protects the down stream equipment, and a gas line to the second gas separator vessel exits at this point. After the check valve, a line from the nitrogen system exits to the back pressure regulator control. The nitrogen line then divides into high- and low-pressure supplies. The high-pressure nitrogen supply is filtered and has a regulator to adjust the operational pressure. The high-pressure line splits again into a gas feed for inside the vessel, and for the purge gas between the liner and the vessel wall. Both lines have mass flow controllers to set flow rates. Check valves and shutoff valves finish the nitrogen feed system. Similarly, the low-pressure line has a mass flow controller to set sweep gas rates, and runs directly to the sweep gas port at the base of the pressure vessel.

The hydrogen and carbon dioxide systems are similar to the nitrogen systems but have a single feed line per gas separator. Regulators set pressure at the manifold and feed line. Mass flow controllers set flow rates. Check valves prevent back flow, and are available to isolate sections of the system. Filters are used to prevent clogging of the regulators and mass flow controllers. Nitrogen for the vessel gas feed joins with hydrogen and carbon dioxide in a single line to the separator vessel. A vent valve and relief valve are close to the vessel to protect the vessel from over pressure. A pressure transducer and a pressure gauge are used to monitor vessel pressure.

There are three exit gas lines from the separator vessel; the feed gas out, the purge gas out, and the sweep gas out. The sweep gas passes through a filter and a rotameter before routing to a gas chromatograph for analysis. The purge gas out passes through a filter and a coil with a double check-valve setup before connecting to the feed gas out. The coil and check-valves allow the pressure to equilibrate on both sides of the liner without excess back-flow of feed gas into the purge system. The feed gas out passes through a filter and join the purge gas prior to being reduced in pressure at a back pressure regulator. The gas then passes through a rotameter and to the gas chromatograph for analysis. The back pressure regulator control panel consists of a nitrogen pressure line and a regulator to set the dome load on the back pressure regulator. The line is filtered and protected with a relief valve and vents.

A schematic diagram of the high-pressure hydrogen separation vessel is shown in Figure 9. The central tube of the vessel (#12) is constructed from oxidation resistant Haynes 230 alloy, and the majority of the other components are made from 316 stainless steel. A bolted rupture disc holder (#1 and #2) with a 1" scored Inconel rupture disc (#3) is located at the top of the vessel. The holder connects to a flange (#8) with a 1-inch I.D. tube entry line for the feed gas (#6 and #7). An alumina liner (#27) is held in the flange with double Viton O-rings (#10). The flange (#8) is bolted to a partner flange (#9) with a spiral wound gasket (#29) between the two. This second flange is welded to the 1-inch I.D. Haynes 230 central tube which has entry (#11) and exit (#13) lines for purge gas. The bottom of the Haynes tube is welded to a third flange (#14) that is bolted to a fourth flange (#15). O-rings (#10) are located in the fourth flange, and secure the bottom of the alumina liner. The feed gas out adapter (#16) is threaded into the fourth flange and provides an exit for the feed gas. A sweep gas in/out adapter (#19) is threaded into the feed gas out adapter. The sweep gas entry tube (#22) passes through the adapter and extends into the ceramic membrane (#26). The exit tube for the sweep gas (#21) is located at the side of the adapter. The ceramic membrane holder tube (#23) is threaded into the sweep gas adapter. The ceramic membrane is coupled to the holder tube using a cup (#24) and a ceramic seal (#25).

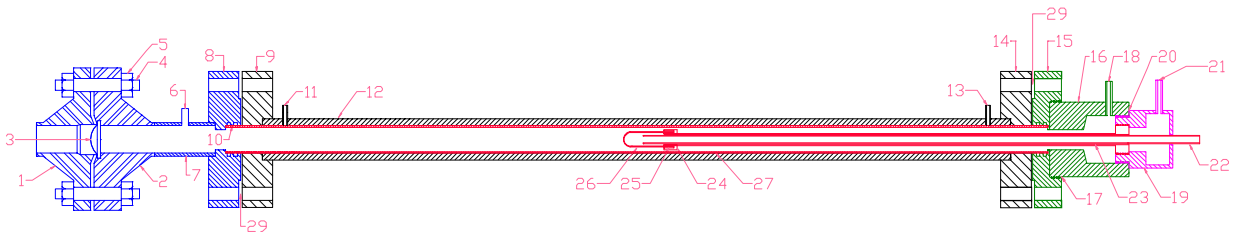


**Figure 9. Diagram for the high-pressure hydrogen separation vessel.**

### g. Hydrogen Transport and Ambipolar Conductivity Measurements and Calculations

The concentration of hydrogen in inlet and sweep streams was determined using a Shimadzu GC 14-A with a Carbosphere 80/100 column (Alltech) and thermal conductivity detection. Argon was used as the carrier gas to maximize sensitivity to hydrogen.

Calculation of hydrogen transport rates, $j_{H2}$, through disk and tube membranes was calculated from,

$$j_{H_2} = \frac{[H_2]F_T}{A} \tag{8}$$

where $[H_2]$ is the hydrogen concentration in the sweep stream, $F_T$ is the total volumetric gas flow from the sweep side of the unit, and $A$ is the membrane surface area (one side only). Ambipolar conductivity, $\sigma_{amb}$, was calculated from transport measurements according to,

$$\sigma_{amb} = j_{H_2} \frac{nFd}{E} \tag{9}$$

where $n$ is the number of electrons per mole of hydrogen, $F$ is the Faraday Constant, $d$ is the membrane thickness, and $E$ is the Nernstian potential across the membrane.

### h. Fabrication of Thin Film Ceramics

During this reporting period, thin film ceramics were prepared by a novel method employing tape casting techniques. The thin films were mixed proton/electron conductors and the substrates were porous disks of the same composition. Using this method, crack-free films on the order of 100 µm thick were achieved.

## RESULTS AND DISCUSSION

### a. Preparation of Ceramic Powders

Tables 1 and 2 contain a summary of preparation conditions and characteristics for several ceramic powders tested during this reporting period. The compositions are represented by H01, H02, etc., and the two-digit appendage indicates the batch number. The materials were perovskite based with the general formula $AB_{1-x}B'_xO_{3-\delta}$. Comparing results for materials H01 (x = 0.05), H02 (x = 0.3), and H04 (x = 0.1) indicated that as the level of dopant increased, there was a decrease in perovskite phase purity. This trend also was observed by comparing lattice parameters of the three materials in Table 2. The lattice parameters were essentially equivalent, which suggested that the perovskite phase contained the same level of transition metal doping, while the remainder of the dopant formed an unidentified second phase.

There was very good agreement between the measured densities listed in Table 1 and the theoretical densities in Table 2. In most cases, the theoretical density was slightly lower than the experimental value due partly to the presence of a second phase. For two-phase samples, the theoretical perovskite density was not representative of the entire experimental sample. The results in the tables suggested that the materials were at least 95% dense, with the exception of H07. The second-phase portion of H07 was too large to make this determination.

**Table 1.**
**Summary of membrane preparation conditions and Characteristics**.

| Material | Calcine Temp. (˚C) | Ave. Particle Size (µm) | Sintering Temp. (˚C) | Sintering Time (hr) | Density ($g/cm^3$) | Phase Purity |
|---|---|---|---|---|---|---|
| H01-01 | 1200 | 0.996 | 1475 | 4 | 6.287 | >98%[1] |
| H02-01 | 1250 | 0.785 | 1475 | 4 | 6.237 | >85%[1] |
| H04-01 | 1225 | 0.439 | 1475 | 4 | 6.126 | >92%[1] |
| H04-03 | 1225 | 0.624 | 1475 | 4 | n/a | >92%[1] |
| H05-01 | 1350 | 0.562 | 1475 | 4 | n/a | 2nd Phase[2] |
| H07-01 | 1300 | 1.073 | 1475 | 4 | 5.588 | 2nd Phase[2] |
| H10-02 | 1250 | 0.612 | 1275 | 6 | n/a | 2nd Phase[2] |

[1] Approximate amount of perovskite phase, remainder is unidentified second phase.
[2] Second phase is an identified additional reaction product in amounts greater than 5%.

**Table 2.**
**Summary of membrane crystallographic data.**

| Material | Analysis State | a (Å) | Theoretical Density ($g/cm^3$)[1] | Second phase [2] |
|---|---|---|---|---|
| H01 | Sintered | 4.393(1) | 6.28 | Minimal |
| H02 | Sintered | 4.394(2) | 6.24 | Unidentified |
| H03 | Sintered | 4.395(1) | 6.18 | Unidentified |
| H04 | Sintered | 4.395(1) | 6.00 | Unidentified |
| H05 | Sintered | 4.188(2) | 6.06 | $K_2NiF_4$, SM |
| H07 | Sintered | Orthorhombic | 5.39 | $K_2NiF_4$, SM |
| H10 | Sintered | 4.399(1) | 6.16 | $ATO_{2.5}$ |

[1] Reported theoretical density of the perovskite phase. Not representative for mixed phase materials.
[2] $K_2NiF_4$ is the parent structure for these second phases, SM = starting material, $ATO_{2.5}$ is a second phase formed between the A-site cation and the transition metal dopant.

### b. Hydrogen Transport and Conductivity of Selected Compositions

At this stage, the focus is on determining the most appropriate experimental conditions for evaluation of hydrogen transport materials. Factors that will influence transport rates, and the ability to systematically evaluate materials, include inlet and sweep gas flow rates, quality of the seal, temperature profile across the cell, catalyst composition and method of application, quality of contact between the catalyst and membrane, membrane thickness and reproducibility, inlet gas humidity, tortuosity within the cell, and length of time to achieve steady state conditions. With this many variables, it is unreasonable to expect that a single set of optimum conditions will be identified early on in the project. Optimal experimental conditions will be discovered as more is learned about the overall system, and the immediate goal is to identify conditions that will enable direct comparisons of materials with a range of compositions. The preliminary data presented below shows promise for ceramic hydrogen separation membranes, and underscores some of the experimental difficulties that must be addressed immediately.

Hydrogen transport data for material H01 are shown in Figure 10. This data was obtained for a 2.4-mm thick disk membrane in the conductivity apparatus using Pt catalyst screen printed on each side of the disk. At temperatures less than 500°C, a steady transport rate of ~0.4 mL/min/$cm^2$ was observed and presumed to be from a leak in the seal. Accordingly, this transport rate was subtracted from the data and results in Figure 10 represent corrected values. The transport rate increased from 0.17 to 1.6 mL/min/$cm^2$ over the temperature range from 638°C to 868°C.

Conductivity data for this sample is shown in Figure 11. There are significant limitations to this technique and the conductivity values likely are underestimated. However, it is anticipated that this method will enable simple and rapid relative comparisons between samples that will facilitate optimizing compositions. The data in Figure 11 was surprising since the electronic conductivity was higher than the ionic conductivity despite having only 5% doping of a transition metal in the B site. The ionic conductivity appeared to level off at higher temperatures, whereas the electronic

conductivity increased sharply. This increase in electronic conductivity at high temperatures likely was responsible for increased transport rates since, in this case, the ambipolar conductivity increased with temperature, *i.e.*, $\sigma_{amb} \rightarrow \sigma_i$ as $\sigma_e \rightarrow \infty$. However, the range of conductivity values obtained from these measurements did not support the observed transport rates. For example, at 638°C a transport rate of 0.17 mL/min/cm$^2$ corresponded to $\sigma_{amb}$ = 0.025 S/cm, compared to $\sigma_{amb} = 4 \times 10^{-5}$ S/cm based on conductivity measurements.

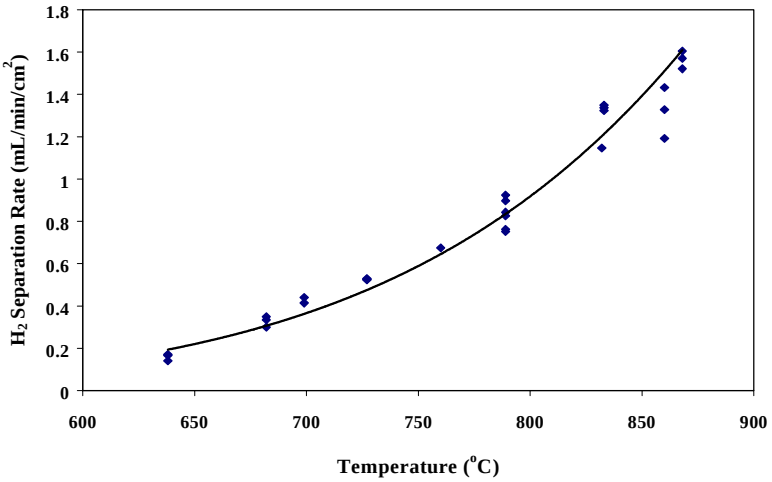


**Figure 10. Plot showing hydrogen transport as a function of temperature for membrane material H01.**

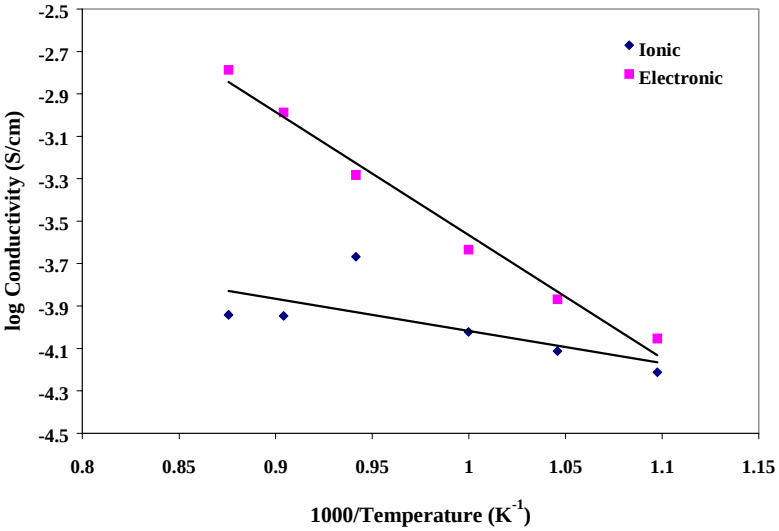


**Figure 11. Plot showing the ionic and electronic conductivity as a function of temperature for membrane material H01.**

As shown in Figure 12, the transport data for sample H02 was much lower than H01. This sample demonstrated a maximum in transport of only 0.024 mL/min/cm$^2$ at 700°C. At higher temperatures the transport rate decreased. Conductivity data is shown in Figure 13, and demonstrated overall higher electronic conductivity than H01. This result was not surprising since the transition metal doping at the B site was 30%. Although these transport rates also did not agree with the conductivity values, the agreement was better than for H01. In particular, the ionic conductivity decreased at higher temperature as did the transport rate, although the temperatures for the decrease did not perfectly correlate. Furthermore, the maximum transport of 0.024 mL/min/cm$^2$ corresponded to $\sigma_{amb}$ = 1x10$^{-3}$ S/cm, compared to 3x10$^{-4}$ S/cm based on measured conductivity. If the conductivity values are to be trusted, it was surprising that the transport rate for H02 was so low compared to H01 considering that both the ionic and electronic conductivity was higher, and the membrane thickness was only 1.3 mm (relative to 2.4 mm for H01).

Sample H04 had an intermediate B-site doping level of 10% and, as seen in Figure 14, this sample demonstrated the highest transport rate. Hydrogen transport increased from ~0.5 mL/min/cm$^2$ at 560°C to ~2 mL/min/cm$^2$ at 740°C. This disk sample was about one half as thick as H01, which might explain the relatively higher transport rate. Acceptable conductivity data was not obtained for this sample. In fact, three samples from different batches generated a wide range of conductivity values. It is not known if the irreproducibility was due differences in batch composition or microstructure, or experimental limitations.

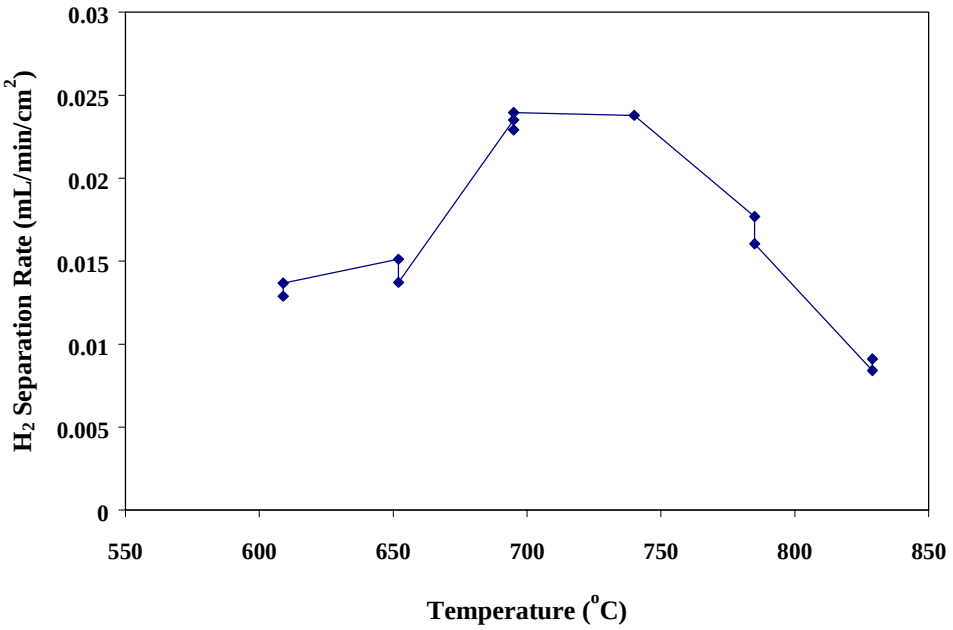


**Figure 12. Plot showing hydrogen transport as a function of temperature for membrane material H02.**

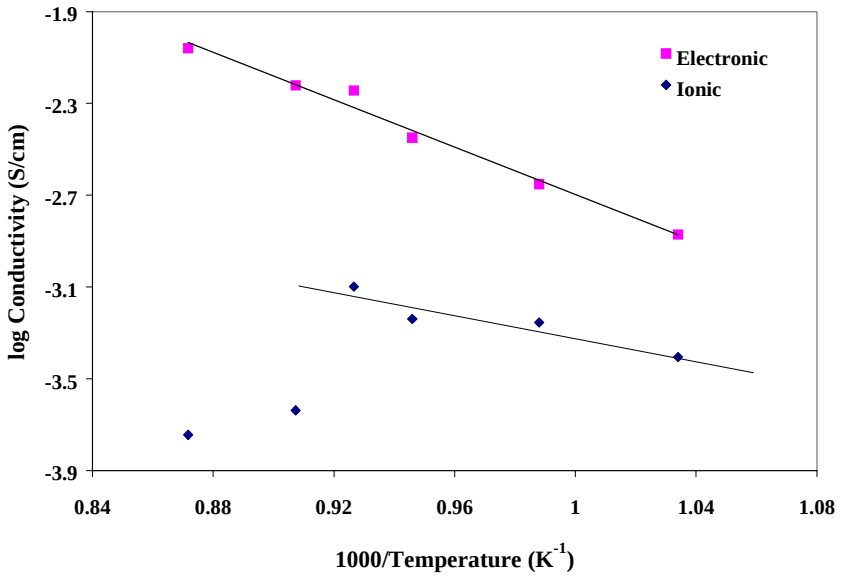


**Figure 13.** **Plot showing the ionic and electronic conductivity as a function of temperature for membrane material H02.**

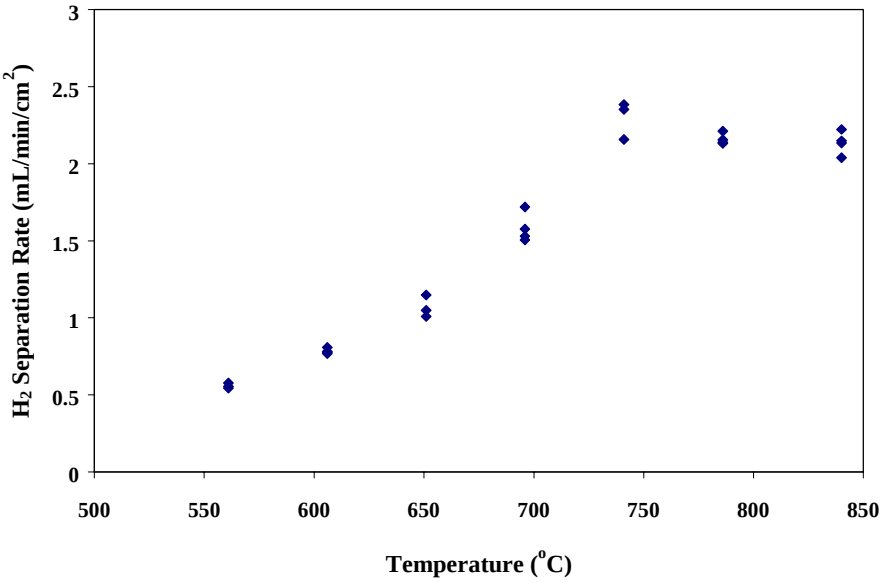


**Figure 14.** **Hydrogen transport as a function of temperature for membrane material H04.**

### c. Problems with Transport and Conductivity Measurements

To date, the major problem associated with hydrogen transport measurements was assessing the extent of leaks in the membrane seal. Originally, carbon monoxide was mixed with hydrogen on the inlet side as a leak check. Although this procedure worked well for large leaks, most leaks were found to be very small and selective against carbon monoxide. For systems with a small leaks in the seal, only hydrogen was observed on the sweep side until the carbon monoxide was replaced with helium. Then, comparable quantities of hydrogen and helium were observed. Helium now is used exclusively for leak check and the only complication is poor chromatographic resolution from hydrogen. This experimental limitation requires switching between gases when doing leak or transport measurements. Leak rates determined from helium permeation can be checked by measuring hydrogen permeation at low temperatures where mixed conductivity does not contribute.

The lack of agreement between the transport and conductivity data also must be addressed. Hydrogen transport to the sweep gas side is very easy to measure chromatographically, and the reliability of the values is based purely on the reliability of the leak evaluation. However, to understand why some materials perform better than other, it is desirable to separate conductivity into the ionic and electronic contributions. The problem is that the current approach does not account for polarization effects of the electrodes, or differences in the interface between the electrodes and different membrane compositions. It was originally anticipated that the current method would be adequate for relative comparisons between materials, but this presumption seems unlikely based on the preliminary data.

### d. Catalysis

Two catalyst systems currently are being used for membrane evaluation. The first was described earlier and consists of a porous platinum film screen printed onto the membrane surface. An SEM image of the catalyst film is shown in Figure 15. The image demonstrates that the platinum was completely interconnected and highly porous. This catalyst adhered very firmly to the membrane surface and is well known to have among the highest activity for the target reactions. The problem is that this system is cost prohibitive, and not considered viable for the final product.

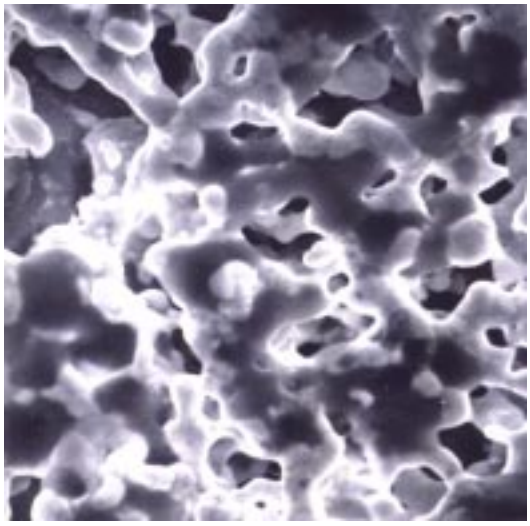

**Figure 15. SEM image of the Pt catalyst screen printed onto a disk membrane. The magnification was 3500x.**

The second catalysts system consisted of the membrane material powder impregnated with nickel metal. A slurry of the impregnated powder was dip coated onto the membrane and calcined. This catalyst system resulted in a rough catalytic surface, however, despite the fact that the powder had the same composition as the membrane, the catalyst adherence was poor. Analogs of this system will be further developed during the next reporting period.

### e. Composite Materials

A range of composite materials were prepared with one ionic conducting ceramic phase and one metallic phase. The metallic phase was varied between 30 and 40% of the total composition. SEM images of these materials revealed distinct metallic regions on the order of 10 µm in diameter. Higher metallic composition resulted in greater connectivity of the metallic phase. During the next reporting period, the effect of particle size will be evaluated, and disk samples will be tested for hydrogen transport.

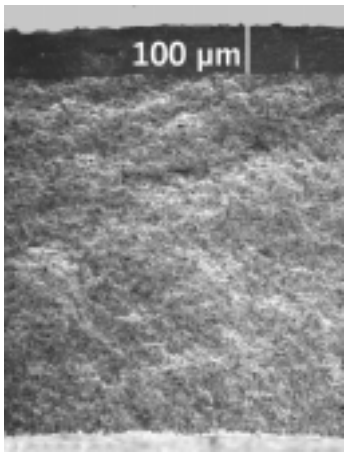


**Figure 16. SEM image (cross section) of a thin perovskite film deposited onto a porous support.**

### f. Thin Films

Thin films of perovskite materials were prepared using tape casting techniques, and an example is shown in Figure 16. This sample demonstrated a homogeneous, crack-free dense membrane supported on a porous substrate of the same composition. The membrane was approximately 100 µm thick, which is typical for tape casting. Spin coating methods will be used to produce films less than 100 µm.

## CONCLUSIONS

Preliminary materials tested in the first reporting period demonstrated a maximum hydrogen transport rate between 1 and 2 mL/min/cm$^2$ for membranes in excess of 1 mm thick. These membrane materials were greater than 95% dense, but the phase purity decreased with increasing dopant concentration. The quantity of dopant incorporated into the perovskite phase was constant, with excess dopant forming an additional phase. Platinum was determined to be an excellent catalyst for evaluating membranes, but due to high cost, alternatives must be developed. The nickel catalyst system tested had poor adherence to the membrane surface. Composite membranes also were successfully prepared with distinct ceramic and metallic phases. It has not yet been determined if the metallic phase was sufficiently interconnected for electron conductivity. Finally, dense ceramic membranes approximately 100 µm thick were successfully prepared using modified tape casting techniques.

## OBJECTIVES FOR NEXT REPORTING PERIOD

Work to be performed during the next reporting period is separated into the following categories:

- Hydrogen transport measurements on doped perovskite tube and disk membranes.
- Hydrogen transport measurements on composite and thin film membranes.
- Comparison of platinum and nickel catalyst systems.
- Assessment of manufacturing issues for perovskite ceramics.